CellPress

Neuron
Article

Sensory Integration in Mouse Insular Cortex Reflects GABA Circuit Maturation

Nadine Gogolla,[1,5] Anne E. Takesian,[2,3] Guoping Feng,[4] Michela Fagiolini,[2] and Takao K. Hensch[1,2,3,*]
[1]Department of Molecular and Cellular Biology, Center for Brain Science, Harvard University, 52 Oxford Street, Cambridge, MA 02138, USA
[2]Department of Neurology, F.M. Kirby Neurobiology Center, Boston Children's Hospital, Harvard Medical School, 300 Longwood Avenue, Boston, MA 02115, USA
[3]Canadian Institute for Advanced Research, 180 Dundas Street West, Toronto ON M5G 1Z8, Canada
[4]Department of Brain and Cognitive Sciences, McGovern Institute for Brain Research, MIT, 43 Vassar Street, Cambridge, MA 02139, USA
[5]Present address: Max Planck Institute of Neurobiology, Am Klopferspitz 18, 82152 Martinsried, Germany
*Correspondence: hensch@mcb.harvard.edu
http://dx.doi.org/10.1016/j.neuron.2014.06.033

SUMMARY

Insular cortex (IC) contributes to a variety of complex brain functions, such as communication, social behavior, and self-awareness through the integration of sensory, emotional, and cognitive content. How the IC acquires its integrative properties remains unexplored. We compared the emergence of multisensory integration (MSI) in the IC of behaviorally distinct mouse strains. While adult C57BL/6 mice exhibited robust MSI, this capacity was impaired in the inbred BTBR T+tf/J mouse model of idiopathic autism. The deficit reflected weakened γ-aminobutyric acid (GABA) circuits and compromised postnatal pruning of cross-modal input. Transient pharmacological enhancement by diazepam in BTBR mice during an early sensitive period rescued inhibition and integration in the adult IC. Moreover, impaired MSI was common across three other monogenic models (GAD65, Shank3, and Mecp2 knockout mice) displaying behavioral phenotypes and parvalbumin-circuit abnormalities. Our findings offer developmental insight into a key neural circuit relevant to neuropsychiatric conditions like schizophrenia and autism.

INTRODUCTION

The insular cortex (IC) is an integral "hub" for dynamic interactions between separate brain networks serving attention and cognition (Kurth et al., 2010). It receives autonomic, visceral, and sensory inputs as part of a "salience network" involved in the detection of novel and relevant information that is collectively upregulated in response to highly stressful experiences (Augustine, 1996; Hermans et al., 2011; Menon and Uddin, 2010; Nieuwenhuys, 2012). The IC is implicated in a wide variety of distinct regulatory, emotional, and cognitive functions. Insular activity increases during subjective awareness of both positive and negative emotions (Bernhardt and Singer, 2012; Caruana et al., 2011; Craig, 2009; Critchley et al., 2004) and in the control and suppression of natural urges (Lerner et al., 2009; Jackson et al., 2011).

An impaired ability to combine sensory input with emotional and cognitive content (Bernhardt and Singer, 2012; Lamm and Singer, 2010) is a primordial feature of social and communication deficits in a variety of neuropsychiatric disorders (Wylie and Tregellas, 2010; Uddin and Menon 2009).

Accordingly, the insula has been consistently identified as a locus of hypoactivity and dysfunctional connectivity in autism spectrum disorders (ASD) and it has been proposed as a brain region of particular interest in understanding the disorder (Di Martino et al., 2009b; Uddin and Menon, 2009). Aberrant multisensory integration (MSI) (Russo et al., 2010; Collignon et al., 2013; Cascio et al., 2012; Megnin et al., 2012) and insular activation (Ebisch et al., 2011; Di Martino et al., 2009a, 2009b; von dem Hagen et al., 2013; Doyle-Thomas et al., 2013; Silani et al., 2008) have been independently linked to autism in human studies. The features of sensory integration in the IC are poorly understood. Notably, robust animal models to probe emergent IC function across development are currently lacking.

Here, we mapped the postnatal maturation of sensory representation and integration in the IC of two inbred mouse strains exhibiting striking differences in core behaviors believed to rely on IC function and to be relevant to ASD. Mice of the BTBR T+tf/J (BTBR) strain display diverse social deficits, impairments in vocal communication, and stereotypic, repetitive behaviors when compared to C57BL/6J (C57) mice (McFarlane et al., 2008; Defensor et al., 2011; Scattoni et al., 2011). In addition to this model of idiopathic autism, we further examined several monogenic mouse models of excitatory-inhibitory (E/I) imbalance, to establish common deficits from diverse etiologies in this neural circuit of particular relevance to neuropsychiatric conditions.

RESULTS

Differential Multisensory Processing in the Insular Cortex of Two Inbred Mouse Strains

Using intrinsic signal imaging of flavoprotein fluorescence (Figures 1A and 1B for experimental setup), we identified partially overlapping auditory and somatosensory response fields in the mouse IC (Figures 1C and 1D), consistent with previous reports

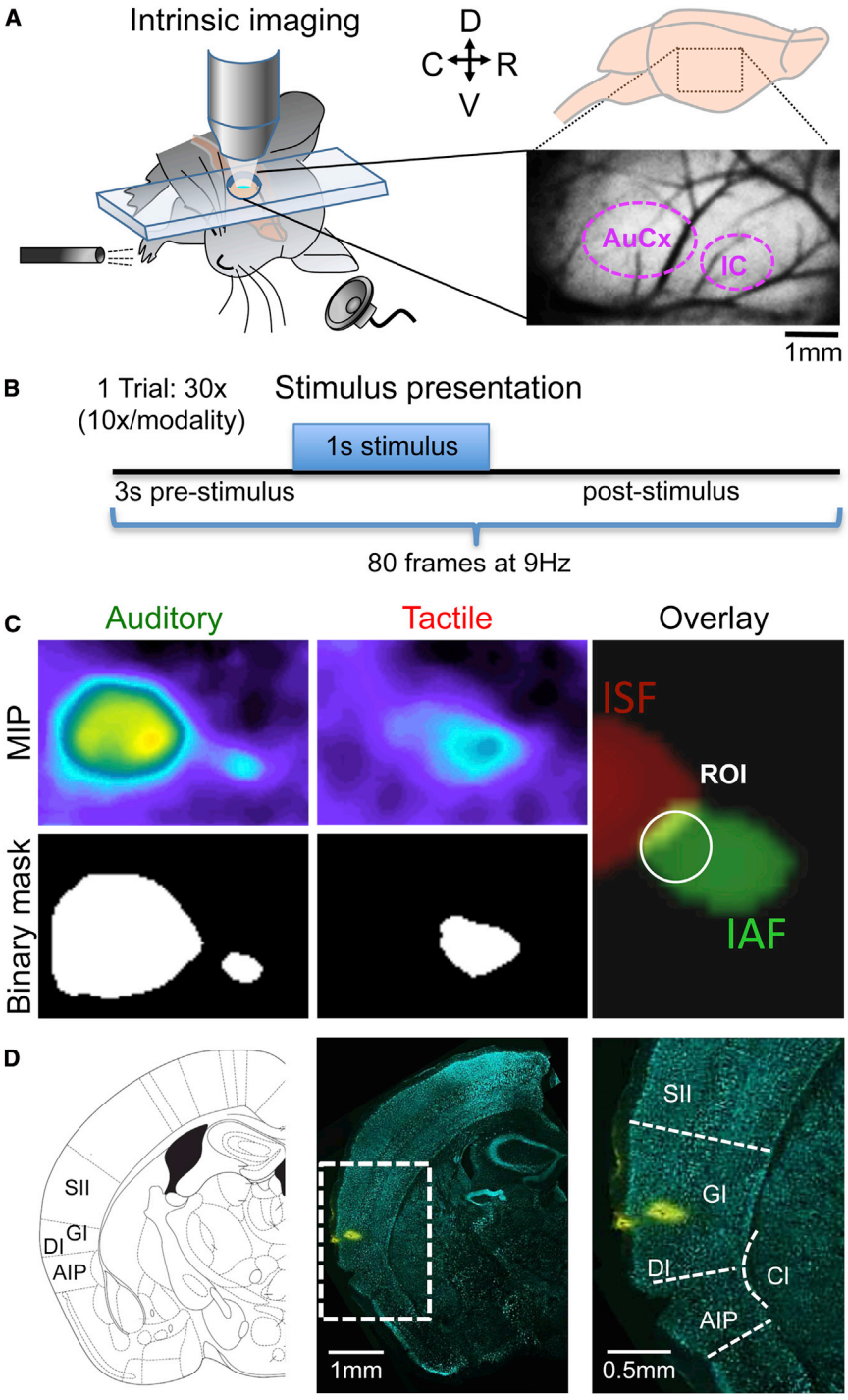

Figure 1. Intrinsic Imaging of Sensory Integration in the Mouse Posterior Insular Cortex

(A) Left: schematic of intrinsic flavoprotein imaging in temporal cortex. Right: field of view (bottom) on the mouse brain (top). D, dorsal; C, caudal; R, rostral; V, ventral. Dotted purple lines demarcate the auditory cortices (AuCx) and posterior insular cortex (IC).

(B) Stimuli for one trial consisted of sets of 30 alternating presentations of auditory, tactile and audio-tactile stimuli (10 each).

(C) Regions of interest (ROI) for MSI measurements. Top left: maximum intensity projections (MIPs) of 35 images following stimulus onset in three to four averaged trials. Bottom left: binary masks of MIPs were created at 15% maximal response constant threshold. Right: overlay of binary masks for the insular somatosensory (ISF) and auditory (IAF) fields. ROIs were placed within the IAF at the interface with the ISF.

(D) Localization of the IAF. Left: schematic drawing of a coronal section at the level of the injection site into IAF (here −1.06 mm from Bregma). Middle: DiI trace within IAF on a Neurotrace (Nissl) stained section. Right: higher magnification of the region in the dotted square. AIP, agranular insular cortex posterior part; Cl, claustrum; DI, dysgranular insular cortex; GI, granular insular cortex; SII, secondary somatosensory cortex.

in the rat and mouse (Rodgers et al., 2008; Sawatari et al., 2011). The insular auditory field (IAF) was readily activated by a wide range of acoustic stimuli ranging from pure tones to complex, naturalistic stimuli such as mouse calls (data not shown). Activation in the insular somatosensory field (ISF) resulted from different tactile stimuli, such as brushing, touching, or an air puff, administered at different positions across the body surface (data not shown) but most prominently at the distal extremities.

To assess multisensory processing in the IC, we compared responses to pure tones of varying sound frequencies and intensities directed to the contralateral ear, air puffs administered to the contralateral front paw, or both audio-tactile stimuli applied concurrently. In response to tones of medium and low sound intensities (60–80 dB sound pressure level [SPL]), adult C57 mice exhibited super-additive multisensory responses in the IAF with amplitudes that were greater than the arithmetic sum of the two sensory modalities applied alone (Figures 2A and 2B).

To quantify the degree of integration, we computed a multisensory index (MI) by dividing the response amplitude upon combined stimulation by the sum of the unisensory responses (Figure 2E). At 60 dB, MI values in C57 mice were generally >100% reflecting super-additivity, while at very high sound intensities (>90 dB SPL), multisensory enhancement was no longer observed consistent with the principle of inverse effectiveness (Figure 2E) (Stein and Stanford, 2008).

In contrast to C57, adult BTBR mice showed neither multisensory enhancement nor apparent integration of the two sensory stimuli regardless of sound intensity (Figures 2A, 2B, and 2E). Notably, at low to medium sound intensities (60–80 dB SPL),

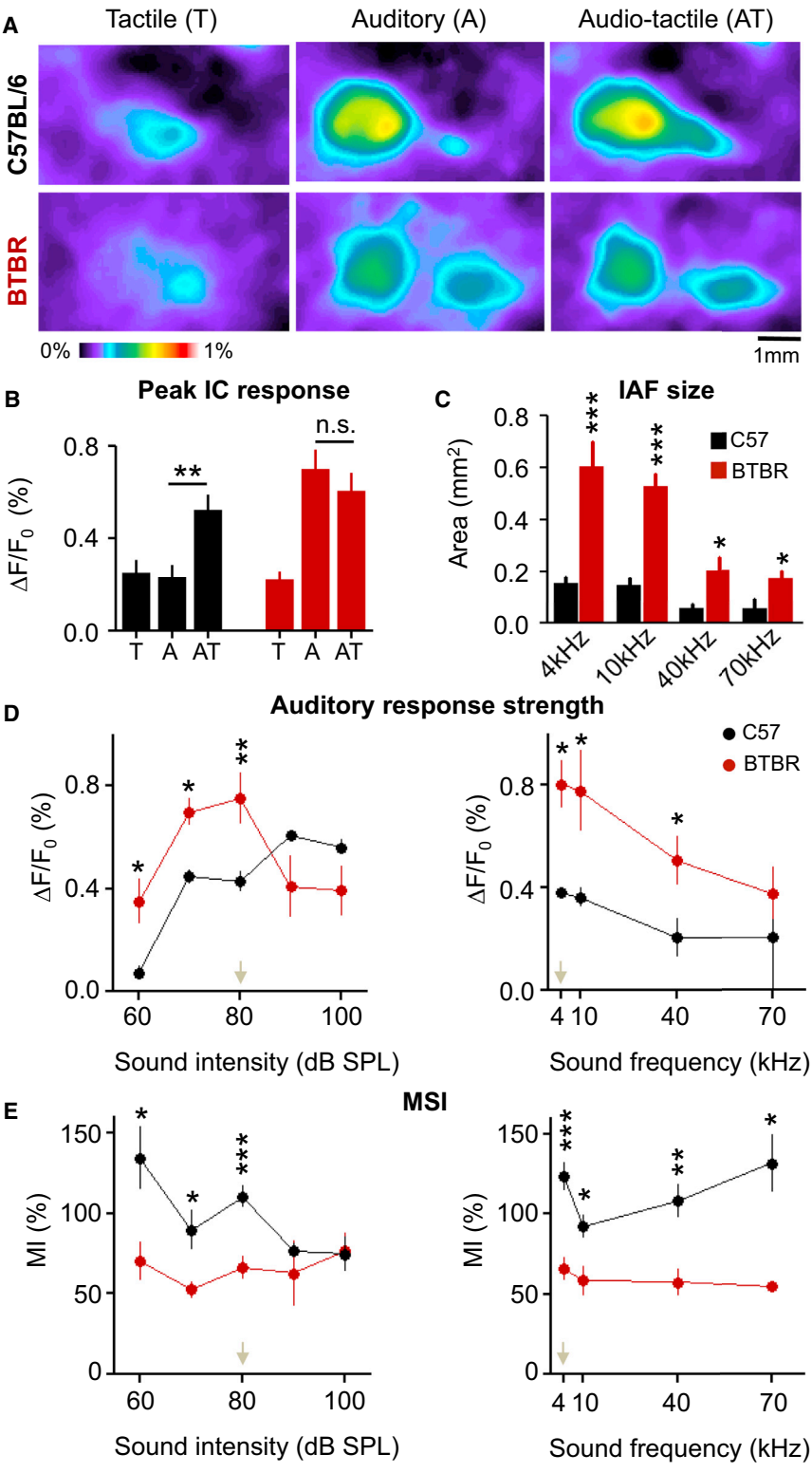

Figure 2. Differential Multisensory Processing in the Insular Cortex of C57 and BTBR Mice

(A) Activation patterns upon tactile (T), auditory (A), and audio-tactile (AT) stimulation in adult C57 (top row) and BTBR mice (bottom row).

(B) Peak response fluorescence (ΔF/F0) in the IC upon A, T, and AT stimulation. AT responses are larger than auditory responses in adult C57 but not in BTBR mice (t test; **$p < 0.01$; n.s. = not significant, $p > 0.05$).

(C) The size of tone activated IC (IAF) is consistently larger in adult BTBR than in C57 mice at different sound frequencies (t test ***$p < 0.001$, *$p < 0.05$).

(D) Peak auditory response strengths upon different sound intensities (left) and frequencies (right) in the IAF. Left: BTBR exhibit significantly larger auditory responses at low to medium sound intensities (≤80 dB) than C57 mice. Right: BTBR mice exhibit stronger auditory responses than C57 across frequencies lower than 70 kHz.

(E) Comparison of MSI expressed as a multisensory index (MI = [AT/(A + T)] × 100) in C57 and BTBR mice. Left: C57 mice adhere to the inverse effectiveness rule as lower sound intensities elicit significantly stronger MSI than higher sound intensities (one-way ANOVA, *$p < 0.05$), while MSI in BTBR mice is equally impaired throughout all sound intensities (one-way ANOVA, n.s., $p = 0.78$). Right: C57 mice exhibit significantly stronger MSI than BTBR mice at all frequencies tested. (t tests; *$p < 0.05$, **$p < 0.01$, ***$p < 0.001$, n.s., $p > 0.05$). All values: mean ± SEM.

BTBR mice exhibited exaggerated auditory responses with a very large portion of IC responding to a pure tone (Figures 2A, 2C, and 2D). Only at very high sound intensities (>90 dB SPL) were auditory responses equally strong in C57 and BTBR mice (Figure 2D).

We next addressed whether multisensory enhancement was frequency-dependent. We found that C57 mice integrated sounds over various frequencies reaching into the ultrasonic range. In contrast, BTBR mice failed to exhibit multisensory integration at all frequencies tested (Figure 2E). Given the dependence of multisensory integration on the intensity of the auditory stimulus, we selected pure tones of medium intensity (80 dB SPL) at 4kHz for the remainder of this study.

Impaired Maturation of Multisensory Integration in BTBR T+tf/J Mice

Sensory integration generally arises through an experience-dependent development (Brandwein et al., 2011; Wallace et al., 2006). We therefore examined the postnatal trajectory of MSI in the IC. In C57 mice, auditory responsiveness was not detectable before postnatal day (P) 14 but became transiently

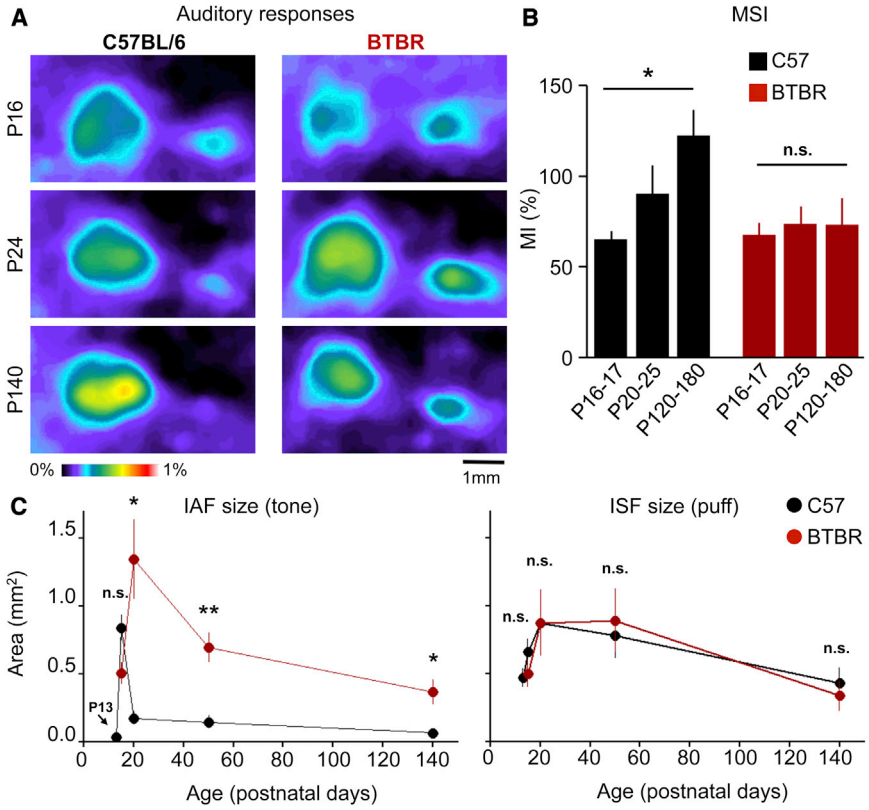

Figure 3. Impaired Maturation of Multisensory Integration in BTBR Mice

(A) With postnatal development, auditory representations contract in the IC of C57 mice but remain enlarged in BTBR mice.

(B) MSI increases with age in the IC of C57 but not BTBR mice. One-way ANOVA (C57: *p < 0.05, BTBR: not significant, n.s.).

(C) Left: insular auditory field (IAF) is rapidly pruned in C57 (no size change >P20) but not in BTBR mice (ANOVA, p < 0.05) whose IAF sizes are significantly larger than in C57 mice at all ages >P20 (t test; *p < 0.05, **p < 0.01). Right: insular somatosensory field (ISF) sizes do not change within each group >P15 (for each, ANOVA p > 0.05) or differ between groups at any age (t tests; p > 0.05). All values are mean ± SEM.

large and widespread around P15/16 (Figures 3A and 3C). Over subsequent days, this response gradually contracted, yielding the characteristically confined IAF of adult C57 mice (Figures 3A and 3C). In BTBR mice, no such rapid postnatal refinement of IAF size was observed. Rather, auditory pruning was greatly prolonged and incomplete (Figures 3A and 3C). Thus, BTBR mice of all ages continued to show an enlarged IAF similar to that observed in juvenile C57 mice at the peak of their postnatal development (Figures 3A and 3C).

Interestingly, the delayed contraction of sensory response field was specific to the auditory map in IC, as tactile stimulation yielded similar ISF sizes in both BTBR and C57 mice at all ages (Figure 3C, right). To monitor developing integration, we then compared MI profiles across groups. The MI was low and not significantly different in juveniles at P16–P17 (Figure 3B). In C57 mice, the MI then gradually increased with postnatal age (Figure 3B) to reach levels of super-additive enhancement (>100%) beyond 2 months of age. In contrast, BTBR mice failed to strengthen IC integration, with similar MI values across all ages (2 weeks–6 months) (Figure 3B). Taken together, these results indicate that impaired postnatal maturation underlies multisensory defects in the IC of adult BTBR mice.

Impaired Integration Reflects Weak Cortical Inhibition in BTBR Mice

Consolidation of unimodal areas, such as primary visual cortex, depends upon the establishment of proper circuit balance (Hensch, 2005). In contrast, autism is associated with E/I imbalance in key brain regions (Rubenstein and Merzenich, 2003; Gogolla et al., 2009). Thus, we examined the expression of inhibitory markers in the IC by immunohistochemistry. In adult BTBR mice, GAD65 puncta were decreased in size, intensity, and density when compared to age-matched C57 mice (Figure 4A). The intensity and number of parvalbumin (PV)+ puncta surrounding NeuN+ pyramidal cell bodies (Figure 4A) were decreased, as was the intensity and complexity of wisteria floribunda agglutinin (WFA)+, perineuronal nets (Figure 4A). These anatomical findings suggest an immature or weakened inhibitory circuitry in the IC of BTBR mice.

To confirm the impact on inhibitory circuit function, we examined miniature inhibitory postsynaptic currents (mIPSCs) recorded in layer (L) 2/3 pyramidal cells of granular insular cortex (GI). While the amplitude of mIPSCs did not differ across strains, the frequencies of these events were significantly decreased in BTBR mice, consistent with a reduction of presynaptic inhibitory innervation (Figure 4B). Instead, miniature excitatory postsynaptic currents (mEPSCs) recorded from GI of BTBR mice displayed no significant changes in amplitude or frequency (data not shown). Acute benzodiazepine agonist treatment (diazepam) enhanced inhibitory transmission in BTBR mice. Bath application (15 μM) prolonged inhibitory currents, producing a significant increase in the mIPSC decay time (not shown) and half-width (Figure 4C).

Given the efficacy of diazepam on mIPSCs in vitro, we asked whether acute administration to BTBR mice in vivo would rescue the observed integration deficits. Systemic diazepam (20 mg/kg intraperitoneally [i.p.]) during multisensory processing as assessed by intrinsic imaging revealed a short-lived restoration of multisensory enhancement lasting 10–20 min (Figure 4D). The same treatment in C57 mice conversely degraded MSI (Figure 4D), indicating that excessive inhibition may equally lead to integration deficits in the IC (see Discussion).

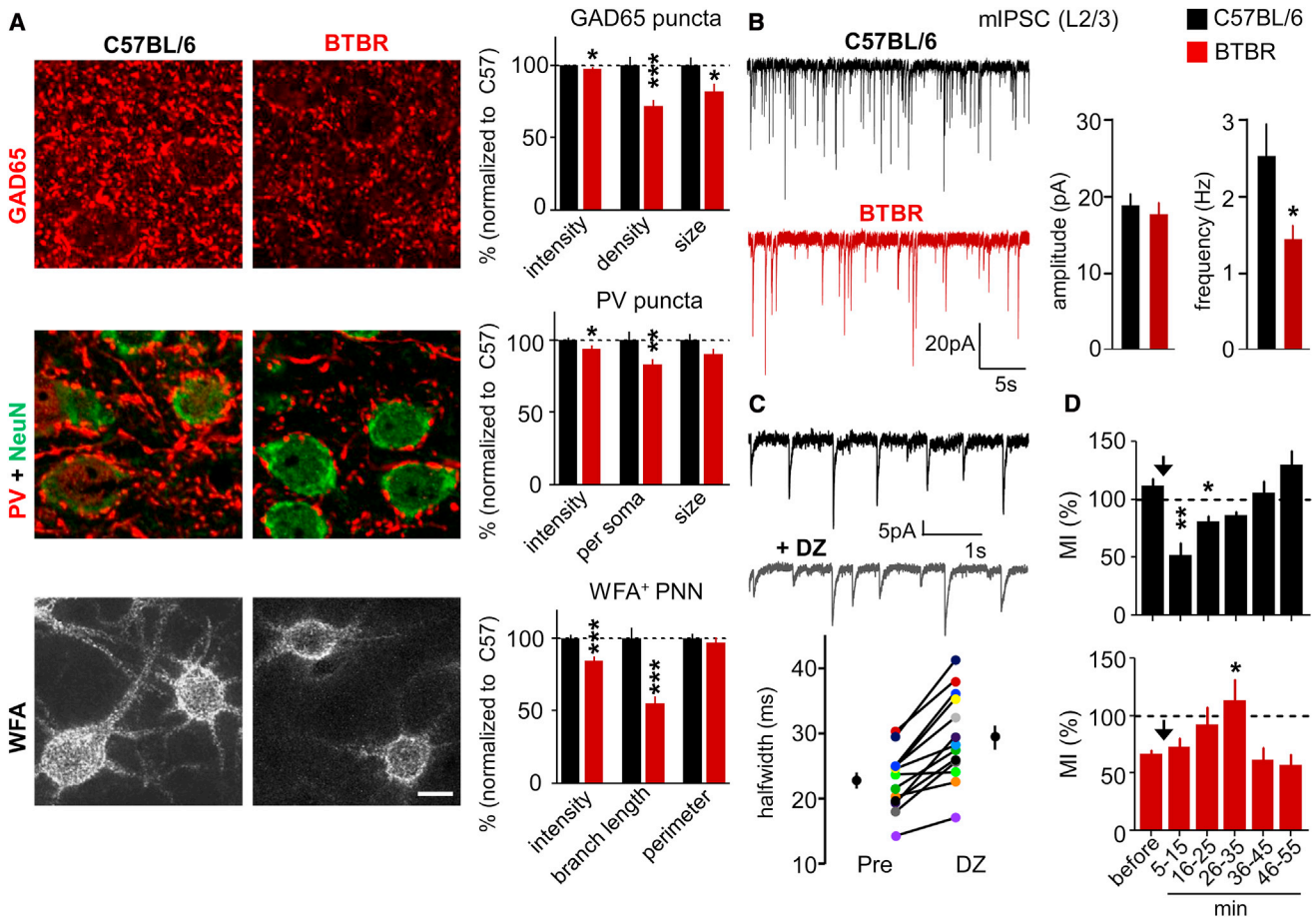

Figure 4. Weak Inhibition Impairs MSI in the IC of BTBR Mice

(A) Decreased expression of inhibitory markers in BTBR mice. Left: representative micrographs of GAD65 (top), PV (middle), and WFA (bottom) immunofluorescence in IC of C57 (left) and BTBR (right) mice. Scale bar represents 10 μm. Right: quantitative analysis of GAD65+ puncta (top), PV+ puncta (middle), and WFA+ perineuronal nets (PNN). All values: mean ± SEM, normalized to C57 (100%).

(B) Miniature inhibitory postsynaptic currents (mIPSCs) recorded in layer (L) 2/3 pyramidal cells of the granular insular cortex (GI) of C57 (black, sample trace top left) and BTBR (red, sample trace bottom left) mice. Note the significant decrease in mIPSC frequency in BTBR mice. C57, n = 17; BTBR, n = 22 cells.

(C) Diazepam (DZ) bath application (15 μM) prolongs inhibitory currents, producing a significant increase in mIPSC half-width and decay time in BTBR mice (top, sample traces before/after DZ; bottom, half-width measures).

(D) Acute DZ treatment in vivo (arrow) yields transient loss of MSI in C57 (black, top), but rescues MSI temporarily in BTBR (red, bottom). Asterisks indicate significant differences from just before injection. All values: mean ± SEM (t test; *$p < 0.05$, **$p < 0.01$, ***$p < 0.001$, n.s., $p > 0.05$).

Rescuing Integration by Early Enhancement of Inhibitory Transmission

Previous work in primary visual cortex has shown that under chronically weak inhibition, an increase of inhibitory transmission by systemic benzodiazepine administration over several days can trigger a critical period of heightened brain plasticity and initiate synaptic reorganization (Fagiolini and Hensch 2000; Hensch 2005). We, thus, hypothesized that boosting γ-aminobutyric acid (GABA) action in BTBR mice over a sustained period might similarly initiate postnatal maturation of MSI and potentially rescue the observed multimodal impairments. BTBR mice were treated for 14 days with benzodiazepine agonist, diazepam (20 mg/kg, i.p. daily) (Fagiolini and Hensch 2000), during one of two time windows (Figure 5A).

First, juvenile BTBR mice were injected during the expected period for IAF pruning (from P15 to P28), when MSI normally would mature in C57 mice (Figures 3B and 3C). Animals were then recorded upon reaching adulthood (P70–P100). Early pharmacological enhancement of inhibition strikingly restored MSI to BTBR mice (Figures 5B and 5C) concomitant with reduced IAF size (Figures 5B and 5D), reflecting an enduring postnatal contraction of auditory response (Figures 5B and 5D). Both MSI strength and IAF size were comparable to C57 mice at P70–P100 (compare Figures 5B–5D and 2C and 2E). Thus, early postnatal inhibitory transmission triggers a refinement of auditory representation and MSI in the IC of BTBR mice.

Second, we treated older BTBR mice with diazepam for a similar duration (P45–P58). Unlike the juvenile group, such a late exposure did not restore MSI or IAF size (Figures 5C and 5D), suggesting an early sensitive period for GABAergic rescue. One possible consequence of juvenile drug treatment may be the permanent rewiring of multisensory circuits in the IC per se.

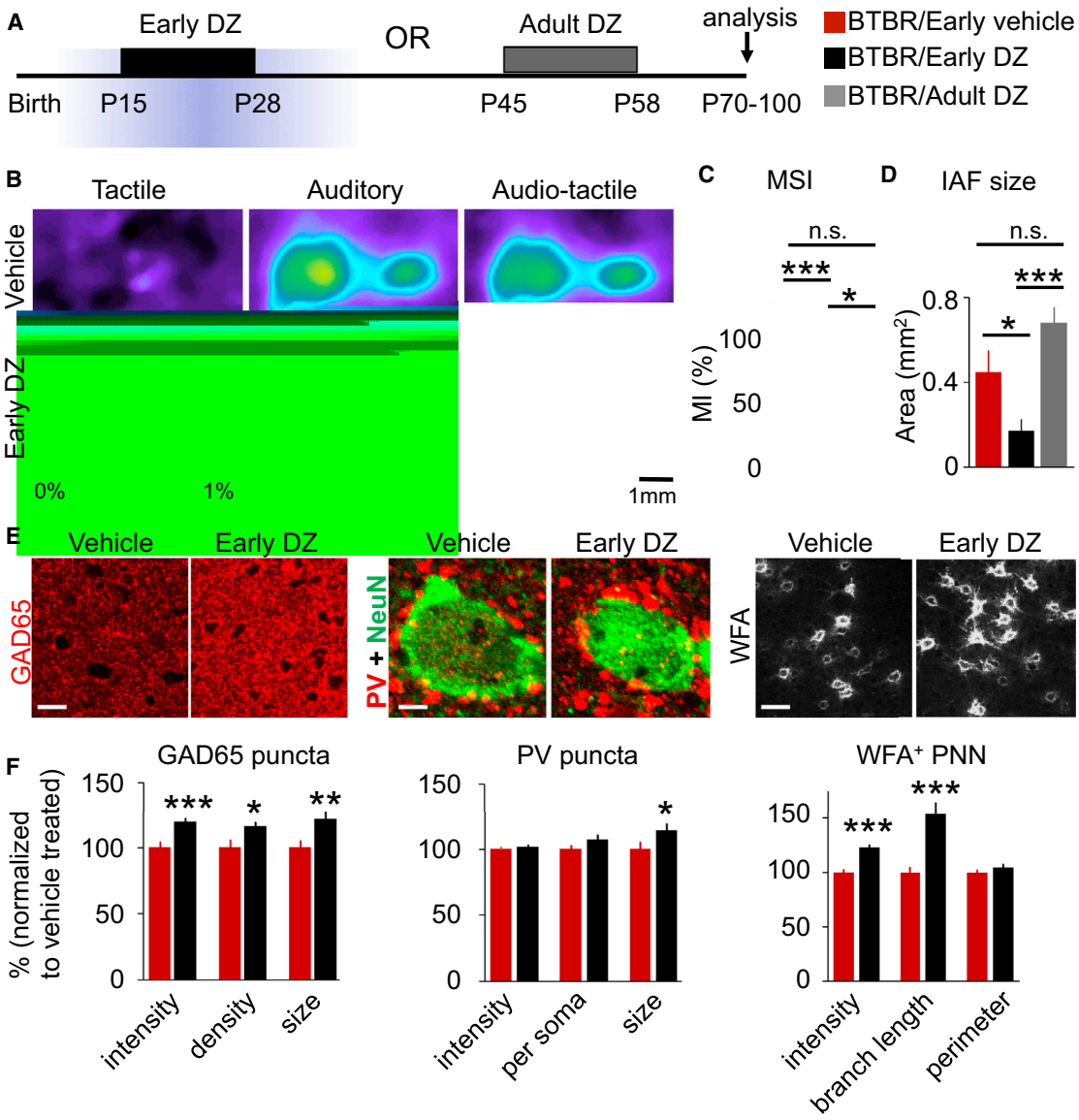

Figure 5. Enhanced Inhibition Early in Life Permanently Rescues MSI in BTBR Mice

(A) Timeline of two diazepam (DZ) protocols in BTBR mice (see Experimental Procedures for details).

(B) Uni- and multisensory responses in treated BTBR mice. Top row: vehicle-treated; bottom row: early DZ-treated. Note decrease in IAF size and rescue of multisensory integration in early DZ-treated animals.

(C) Increased MSI by early DZ treatment as compared to adult DZ treatment or early vehicle treatment.

(D) IAF size restricted significantly after early (but not adult) DZ treatment.

(E) Early DZ rescues inhibitory markers in the IC of BTBR mice: immunohistochemistry against GAD65+ (left), PV+ puncta around NeuN+ somata (middle), and WFA+ perineuronal nets (PNN) (right) after early vehicle or DZ-treatment. Scale bars represent 20 μm (left), 4 μm (middle), and 30 μm (right).

(F) Quantitative analysis of GAD65+ puncta intensity, density and size (left), PV+ puncta intensity, number per NeuN+ soma and size (middle), PNN intensity, branch length, and perimeter (right). All values: mean ± SEM, normalized to vehicle control (100%) (t test: *$p < 0.05$, **$p < 0.01$, ***$p < 0.001$, n.s., $p > 0.05$). See also Figure S1.

Establishment of proper E/I balance that outlasts early drug exposure has been shown in the primary visual cortex (Fagiolini and Hensch 2000; Iwai et al., 2003). Thus, we reexamined inhibitory marker expression in the IC of adult BTBR mice treated with diazepam as juveniles. Size, density, and intensity of GAD65 puncta were significantly rescued in adulthood (Figures 5E and 5F). Likewise, PV+ puncta (basket synapses) around NeuN+ pyramidal cell bodies had increased in size (Figures 5E and 5F) and WFA+ perineuronal nets exhibited greater intensity and complexity (Figures 5E and 5F).

These findings reveal that a transient increase of inhibition in early postnatal life induces an enduring inhibitory circuit

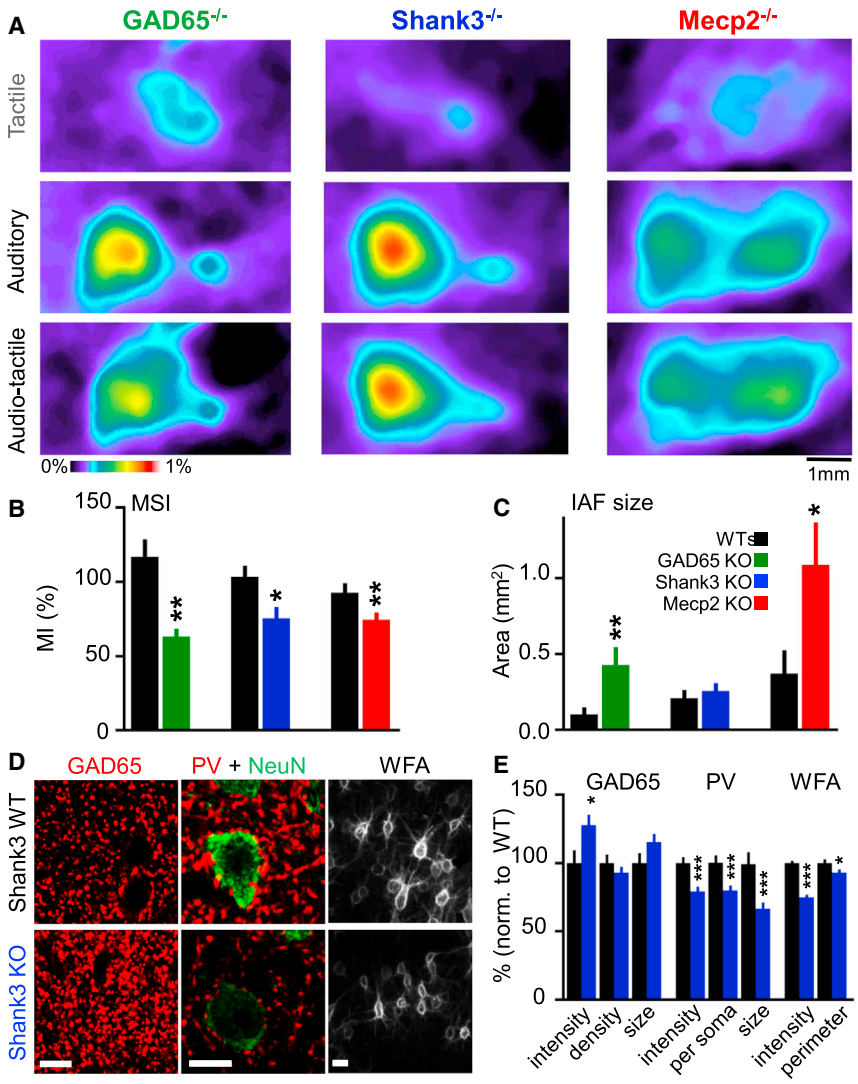

Figure 6. Shared Multisensory Integration Deficits across Monogenic Mouse Models of Autism

(A and B) Tactile, auditory, and audio-tactile responses in GAD65, Shank3, or MeCP2 knockout (KO) mice (A) and their impaired MSI (B).

(C) Adult IAF sizes are enlarged in GAD65 and Mecp2 KO mice, but remain unaltered by deletion of Shank3.

(D and E) Immunostaining for GABA markers in the IC of Shank3 KO animals exhibits (D) increased intensity of GAD65 puncta (E), while the intensity, number per pyramidal cell soma, and size of PV puncta is decreased, as are WFA+ PNN size and intensity, compared to wild-type. Scale bars represent 10 μm. All values: mean ± SEM (t test; *$p < 0.05$, **$p < 0.01$).

See also Figure S2.

reorganization and proper multisensory processing in the IC of adult BTBR mice. The same early treatment interestingly reduced the amount of self-grooming behavior as well (Figure S1 available online).

Monogenic Models of Autism Share MSI Deficits in the Insular Cortex

Our results with BTBR mice suggest that impaired sensory integration may arise from altered neurodevelopmental trajectories of E/I balance, consistent with a widely held view of autism spectrum disorders (Rubenstein and Merzenich, 2003; Gogolla et al., 2009). To ascertain the generality of the IC defect, we assessed MSI in three etiologically distinct mouse models of E/I imbalance, which do not harbor the many homozygous mutations and developmental defects that are common to inbred mouse models such as the acallosal BTBR strain.

First, we tested direct genetic perturbation of inhibitory circuits in mice lacking GAD65, one of the two major enzymes synthesizing the inhibitory neurotransmitter GABA. Adult GAD65 knockout (KO) mice exhibited large IAFs and impaired MSI (Figures 6A and 6B). Notably these mice also displayed autism-relevant behaviors, such as excessive self-grooming and impaired social approach (Figure S2). Thus, loss of GAD65 itself leads to MSI deficits in the IC and the expression of autism-like behaviors.

In humans, disruptions of the Shank3 gene are linked to 22q13 deletion (Phelan-McDermid) syndrome and other non-syndromic ASDs (Durand et al., 2007). Recently, it has been shown that mice with Shank3 gene deletions exhibit autistic-like behaviors (such as hyper-grooming) together with reduced cortico-striatal synaptic transmission (Peça et al., 2011). Here, we found that Shank3 KO mice also display MSI deficits in the IC (Figures 6A and 6B). Unlike BTBR mice, IAF sizes were not altered in Shank3 KO as compared to wild-type mice (Figure 6C), indicating that MSI deficits are not purely a consequence of auditory hyperresponsiveness. Rather, PV+ puncta and WFA+ perineuronal nets were again found to be compromised in these animals (despite a global increase in GAD65+ puncta) (Figures 6D and 6E), suggesting that functional connectivity of PV-circuitry may be most relevant for MSI.

To explore this possibility further, we finally addressed MSI in mice lacking the methyl-CpG- binding protein 2 (Mecp2) that display an early hypermaturation of perisomatic PV-circuits but overall decrease in GAD65 and subsequent regression of cortical function as they grow older (Durand et al., 2012). Based on mutations found in human patients, Mecp2 KO mice serve as a model for Rett syndrome and several other neurodevelopmental disorders including cognitive disorders, autism and juvenile-onset schizophrenia (Moretti and Zoghbi, 2006). Despite presenting the opposite combination of inhibitory circuit perturbation found in the absence of Shank3, Mecp2 KO mice also

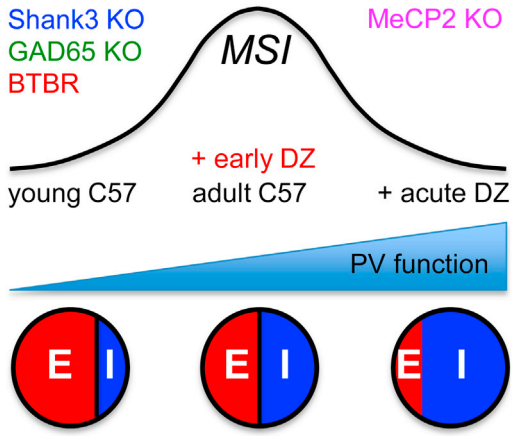

Figure 7. Optimal Range of PV Circuit Function Underlies MSI in the IC

Multisensory integration in the IC reflects an optimal E/I circuit balance, in particular that of PV circuit function. Pharmacological or genetic manipulations which excessively weaken or strengthen PV-circuit function disrupt MSI in the adult insula.

exhibited impaired MSI in the IC (Figures 6A and 6B) along with an extremely large IAF reminiscent of those observed in BTBR mice (Figure 6C). Taken together, an optimal range of PV-circuit function may be required for integration in the mature IC to emerge (Figure 7).

DISCUSSION

Our study reveals that the postnatal emergence of integrative properties in the IC relies on the maturation and strengthening of inhibitory circuits. We further show that four distinct ASD mouse models of unrelated etiologies, but characterized by disrupted E/I balance, exhibit a common phenotype of impaired sensory integration. Importantly, our results suggest an optimal range of PV cell function in particular may enable proper MSI in the IC.

Integration in the IC as a Model to Understand ASD Mechanisms

Aberrant function in higher order brain regions may reflect circuit development locally, the cumulative impact of prior unimodal stages or both (Hensch, 2005). It is likely that multiple brain areas, rather than any one site, contribute to the complex manifestations of autism (von dem Hagen et al., 2013, Uddin and Menon, 2009). The IC is well-suited to investigate the dynamic interactions and basic principles of this integration across large-scale networks processing sensory, visceral, emotional, and cognitive information (Menon and Uddin, 2010). Our initial characterization of MSI development in the mouse IC then provides an excellent model system for investigating the relationship between microcircuits and distant input.

This structure combines features consistently impaired in human autism, such as long-range disconnection, local E/I imbalance, and sensory hyperresponsiveness (Courchesne and Pierce, 2005; O'Neill and Jones, 1997; Rubenstein and Merzenich, 2003). Notably, gastrointestinal problems are often comorbid with ASD (Chaidez et al., 2014; Hsiao et al., 2013; Mazurek et al., 2013; McElhanon et al., 2014), which may send strong, persistent visceroceptive signals to the IC. Finally, the proposed roles of the IC in emotion and cognition make it an ideal candidate region underlying critical aspects of neuropsychiatric disorders more broadly, such as social behaviors, ranging from self-awareness to empathy (Craig, 2009; Engen and Singer, 2013). Moreover, safety signals that predict stress-free periods are learned in the posterior IC (Christianson et al., 2008).

In this context, it may be noteworthy that integration of auditory and forepaw tactile stimulation was disrupted in our animal models. The contingency of these inputs is salient during rough-and-tumble play behaviors, especially during social development in rodents (Panksepp, 1981). The pruning of hyperresponsive auditory regions within the IC was normally found to occur just ahead of this period of intense play behavior, but failed to do so in BTBR mice (Figure 3). The latter engage in numerous bouts of stereotypical self-grooming behaviors (Figure S1) and lower levels of spontaneous, conspecific social interactions in the home cage environment throughout juvenile development (Babineau et al., 2013; McFarlane et al., 2008; Pearson et al., 2011). It is then interesting that somatosensory activation of the IC follows a normal developmental trajectory in BTBR mice, while the maturation of auditory response is aberrant (Figure 3). Given their subadditive response to conjoint stimulation, self-grooming in these mice may serve to blunt the excessive (potentially "painful") activation of the IC by ambient sound or internal inflammatory cues (Onore et al., 2013).

In contrast, language—that is classically disrupted in ASD patients (Uddin and Menon, 2009; Silani et al., 2008)—is a quintessential sensory integration task (Gick and Derrick, 2009) potentially involving the IC (Remedios et al., 2009; Habib et al., 1995; Allen et al., 2008; Ackermann and Riecker, 2010). Hypoactivity, altered size, and reduced functional connectivity in the IC have repeatedly been reported along with MSI deficits in autistic patients (see Introduction) (Di Martino et al., 2009b). Here, we found that ultrasonic vocalizations also activate the IC in mice (data not shown), but to what degree this is reduced in BTBR mice exhibiting a limited and unusual repertoire of vocalizations (Scattoni et al., 2011) remains to be explored.

Parvalbumin Circuit Function and MSI in the IC

Our data further suggest that diverse genetic alterations in microcircuit function can lead to common IC deficits in integration. Anatomical evidence suggested that the salient component of this E/I balance involves the status of PV-circuits. When they are weakened (BTBR, Shank3 KO, GAD65 KO) or hyperconnected (Mecp2 KO) (Durand et al., 2012), MSI in the IC is impaired. Similarly, in young C57 mice whose PV-circuits are still maturing, weak MSI gradually strengthens with increasing postnatal age. Degradation of MSI in adult C57 mice acutely injected with diazepam (Figure 4D) further corroborates the idea of an optimal range for PV-cell function governing MSI (Figure 7).

Notably, the same acute treatment temporarily improved MSI in adult BTBR mice (Figure 4D), and enduringly, concurrent with increased PV puncta size, when applied over several days in early life (Figure 5).

What might determine the optimal range of PV-cell function underlying MSI? Recent work in the mouse visual cortex offers a clue. Unlike pyramidal cells that exhibit enhanced visuo-tactile response, very little increase in firing is observed in PV-cells to multisensory versus unimodal stimulation (Olcese et al., 2013). Thus, during multimodal stimulation, pyramidal cells may receive proportionally less inhibition from their surrounding PV-cells than for unimodal stimulation. This could provide a mechanism by which excessive PV circuit function might disrupt MSI on a population level. Indeed, optogenetic activation of PV cells impairs enhancement in neighboring pyramidal cells (Olcese et al., 2013). Likewise, weak PV circuit function may fail to adequately dampen pyramidal cells during unimodal input to allow for substantial firing increases upon multimodal stimulation. This optimal PV circuit function model (Figure 7) underlying MSI can now be tested directly by targeted optogenetic activation or silencing of PV-cells in the IC.

Acute amelioration of autism relevant behaviors by benzodiazepine treatment in adult BTBR mice has been reported for social interactions (Defensor et al., 2011; Han et al., 2014), repetitive behaviors, and spatial learning (Han et al., 2014). In accordance with our MSI results, the effect of adult diazepam treatment in these studies is not long lasting (Han et al., 2012). In contrast, our study suggests that early treatments aimed at restoring E/I balance during developmental windows of circuit maturation may provide the potential for long-term improvements of autistic phenotypes. Our treatment was sufficient to permanently increase the size, density, and intensity of GAD65 puncta, size of PV puncta, and intensity and branch length of PNNs, indicating a permanent strengthening of local inhibitory circuits. We could further demonstrate that excessive grooming behavior in adult BTBR mice was enduringly improved through this early diazepam treatment (Figure S1), but other autistic behaviors remain to be tested.

In the adolescent brain, GABA signaling itself can powerfully regulate PV cell innervation patterns (Chattopadhyaya et al., 2007). Decreased GABA levels in basket interneurons impair axon growth and bouton formation during the postnatal maturation of perisomatic innervation, while boosting the $GABA_A$ receptor function with diazepam rescues these defects under low GABA availability, but not under control conditions (Chattopadhyaya et al., 2007). In our study, treating juvenile BTBR mice with diazepam may similarly induce proper maturation of perisomatic inhibition by PV cells and thus permanently increase PV circuit connectivity, ultimately rescuing MSI function in adulthood. Why the same acute treatment is not long-lasting in adult BTBR mice is unclear. Perhaps the level of GABAergic transmission, albeit lower than in C57 mice, is still sufficient to close a critical period of plasticity in earlier stages of the sensory hierarchy leading up to the IC, thus preventing the same extent of network remodeling observed when treating juvenile mice.

Alternatively, the role of local PV cells in pruning long-range thalamocortical afferents to primary sensory areas offers another possibility (Hensch, 2005). Recent anatomical evidence reveals topographic projections from the auditory thalamus (MGv) directly into the IC (Takemoto et al., 2014). As PV cell-mediated inhibition within the IC matures, activity-dependent pruning of these inputs may be enabled, much as for tonotopic or ocular dominance maps in auditory and visual cortices, respectively (Barkat et al., 2011; Hensch and Stryker, 2004). In BTBR mice, this developmental pruning specifically of auditory input may fail to occur due to inadequate PV-cell function, but rescued during a critical period by diazepam.

MSI Disruption across Multiple ASD Models

One of the major findings of our study is that MSI deficiencies are found in the IC of several ASD models of differing etiology. Animal studies have offered many possible genetic, cellular, and circuit mechanisms that underlie particular deficiencies, but only few have addressed commonalities between them. This stands in stark contrast to work with human patients, where the etiology of the disorder is often unknown and thus different subtypes of ASD are grouped together. The choice of BTBR, Shank3 and Mecp2 lines here is representative of three distinct clusters identified by MRI-based neuroanatomical phenotyping of 30 different ASD mouse models (Ellegood et al., 2013).

Across groups, when PV-circuits in the IC appear weak, MSI was compromised. This was true not only in adult BTBR mice, young wild-type or following direct GAD65 deletion, but also after the delayed compensatory reduction of GAD65 in Mecp2 KO mice which display an early PV-circuit hyperconnectivity (Durand et al., 2012). We surprisingly also found diminished PV puncta in the adult IC lacking Shank3, a key regulator of the postsynaptic density at glutamatergic synapses. The precise location of the mutation within the Shank3 gene is key to its phenotypic outcomes (Han et al., 2013; Kouser et al., 2013; Wang et al., 2011; Yang et al., 2012). These reflect defects specific to discrete brain regions rather than an overall CNS dysfunction, such as corticostriatal glutamatergic signaling in our Shank3 KO mice that may underlie their obsessive grooming (Peça et al., 2011). Our results here further implicate altered GABA circuits in the IC underlying their asocial urges. Acute direct manipulation of PV-cell function (e.g., optogenetic activation/silencing) as well as single-unit recording in the mature IC will be informative.

The trajectory of PV-circuit maturation also determines timing of critical period plasticity (Hensch, 2005). Pruning of the IAF is no exception: either a delayed (BTBR, GAD65 KO) or accelerated time course of PV-connectivity (Mecp2 KO) preserves a broad, immature auditory response in the IC. Instead, normal IAF size in adult Shank3 KO mice suggests that their PV-cell deficits in the IC arise late after the critical period for auditory pruning has passed. It further reveals that MSI and absolute IAF size are dissociable. What appears crucial for MSI to emerge is an optimal E/I balance by PV-circuits in adulthood. Notably, our results suggest a therapeutic strategy in development to permanently correct mechanisms relevant to autism through GABA manipulation in early postnatal life. As these early treatments may induce enduring circuit rearrangements, they will need to be carefully tailored to the low/high PV status of individual ASD etiologies. Identifying a key neuronal circuit that is disturbed across subgroups of the disorder is an essential first

step to assess treatment success or as a novel biomarker for early detection.

EXPERIMENTAL PROCEDURES

See a detailed description in the Supplemental Experimental Procedures.

All procedures were conducted in strict compliance with the institute's Guidelines for the Care and Use of Laboratory Animals of Harvard University. Founder C57BL/6J and BTBR T+tf/J mice were purchased from Jackson Laboratory. Original GAD65 KO breeders obtained from Dr. K. Obata (RIKEN BSI), Shank3 KO adults from G. Feng (MIT), and Mecp2 KO breeders from Jackson Laboratory (B6.129P2(c)-Mecp2$^{tm1.bird}$/J) and bred in house on a 12 hr light/dark cycle with food and water available ad libitum. All control animals were WT age-matched littermates of mutant mice. We used on average greater than five (and at least three) mice per condition.

In Vivo Intrinsic Imaging

Imaging of intrinsic flavoprotein fluorescence from insular cortex in vivo (Figure 1A) was performed under Nembutal (50 mg/kg for adult mice; 25 mg/kg for animals <P25) and Chlorprothixene (0.25 mg/kg for adult mice; 0.1 mg/kg for mice <P25 days) anesthesia as described in Shibuki et al. (2003). For tactile stimulation, airpuffs (1 s, 25 psi) were produced with a Picospritzer III (Parker) and directed through a small plastic tube (1.5 mm inner diameter) onto the inside of the contralateral frontpaw. For auditory stimulation, pure tones of different frequencies and intensities were generated (System3, Tucker Davis Technologies) and presented (1 s) from an electrostatic speaker (ES1, TDT) mounted in front of the contralateral ear. Multisensory stimulation was simultaneous presentation of both stimuli.

Quantitative Analysis of Intrinsic Fluorescence Signals

One trial consisted of 30 stimulus repetitions: 10 for each modality, alternating auditory, tactile, and multisensory (both). For each stimulus repetition, a time stack was acquired (80 image planes at 9 Hz). Stimuli (1 s) were presented after a 3 s prestimulus period (Figure 1B). Time stacks for each trial were acquired, processed, and analyzed using Metamorph software (version 7.1.1.0, 2007). For each mouse, images were averaged of the same stimulus modality from three to four trials. Fluorescence intensities were measured within two circular regions of interest (ROIs, 0.2 mm radius). One control ROI was positioned at the periphery in a region that showed only background fluorescence fluctuations (on bone or skin). The second ROI was placed manually within the IAF caudal extreme, adjacent to ISF, guided by a binary mask of activated regions (see Figure 1C). Signal intensities recorded within these ROIs and fluorescence changes in the IAF were calibrated by subtracting control ROI intensities. Change in IC fluorescence intensity upon stimulation ($\Delta F/F0$) was calculated by dividing the calibrated response (ΔF) by the averaged intensity over the first 24 frames before stimulus onset (F0). Peak responses were averages over 8 frames (~890 ms) around maximal $\Delta F/F0$ values. Strength of integration was expressed as multisensory integration index, MI = [AT] × 100/([A] + [T])], where [AT] = peak multisensory, [A] = peak auditory, and [T] = peak tactile responses. To best depict qualitatively the position and extent of cortical activation upon sensory stimulation, images shown in Figures 1C, 2A, 3A, 5B, and 6A are maximum intensity projections (MIPs) of 35 frames (3.8 s) following stimulus onset taken from the averages of three to four trials. All data analysis was performed using Metamorph software and custom MATLAB scripts.

Immunohistochemistry

Coronal brain sections were stained with one of the following antibodies: mouse anti-GAD65 (1:1,000, Millipore); rabbit anti-PV (1:500; Swant); mouse anti-NeuN (1:100, Millipore); *Wisteria floribunda* lectin (1:200, Vector Laboratories). Images within the IC were acquired on a confocal microscope (Olympus) and analyzed using ImageJ software.

In Vitro Electrophysiology

To evaluate functional synaptic inhibition, whole-cell recordings (Axopatch 1D; Axon Instruments) were obtained from pyramidal neurons in granular IC layers (L) 2/3.Effects of acute diazepam on mIPSCs were recorded 15 min following bath application.

Diazepam Treatment

Chronic diazepam (20 mg/kg in 0.9% saline) was administered daily (i.p.) for 14 days between P15–P28 for early and P45–P58 for late treatments, respectively. Acute treatments consisted of a single dose during the imaging session.

Statistical Analysis

All data presented as mean ± SE with n and ages as shown in figures or stated in text. All data were first analyzed for D'Agostino and Pearson omnibus normality. The following parametric tests were used: one-way ANOVA with Tukey's multiple comparison test for comparison of multiple groups, two-way ANOVA for comparing MSI development, and unpaired t test for comparing between two groups. The following nonparametric tests were used: Mann-Whitney rank-sum test for comparing between two groups.

SUPPLEMENTAL INFORMATION

Supplemental Information includes Supplemental Experimental Procedures and two figures and can be found with this article online at http://dx.doi.org/10.1016/j.neuron.2014.06.033.

AUTHOR CONTRIBUTIONS

N.G. performed in vivo imaging, anatomy, and behavior. A.E.T. performed in vitro slice electrophysiology. G.F. and M.F. provided mice and discussion. N.G. and T.K.H. designed the study and wrote the paper.

ACKNOWLEDGMENTS

We thank M. Nakamura for animal care, M. Ho for help with behavioral tests and T.K.H. laboratory members for feedback and discussion. Funded by the National Institute of General Medical Sciences (NIGMS) (DP1OD003699 to T.K.H.) and the National Institute of Mental Health (NIMH) (1P50MH094271 to T.K.H.), as well as postdoctoral fellowships from the Human Frontier Science Program (HFSP) and Charles King Trust/Charles Hood Foundation (to N.G.) and the Nancy Lurie Marks Foundation (to A.E.T.).

Accepted: June 24, 2014
Published: July 31, 2014

REFERENCES

Ackermann, H., and Riecker, A. (2010). The contribution(s) of the insula to speech production: a review of the clinical and functional imaging literature. Brain Struct. Funct. *214*, 419–433.

Allen, J.S., Emmorey, K., Bruss, J., and Damasio, H. (2008). Morphology of the insula in relation to hearing status and sign language experience. J. Neurosci. *28*, 11900–11905.

Augustine, J.R. (1996). Circuitry and functional aspects of the insular lobe in primates including humans. Brain Res. Brain Res. Rev. *22*, 229–244.

Babineau, B.A., Yang, M., Berman, R.F., and Crawley, J.N. (2013). Low home cage social behaviors in BTBR T+tf/J mice during juvenile development. Physiol. Behav. *114-115*, 49–54.

Barkat, T.R., Polley, D.B., and Hensch, T.K. (2011). A critical period for auditory thalamocortical connectivity. Nat. Neurosci. *14*, 1189–1194.

Bernhardt, B.C., and Singer, T. (2012). The neural basis of empathy. Annu. Rev. Neurosci. *35*, 1–23.

Brandwein, A.B., Foxe, J.J., Russo, N.N., Altschuler, T.S., Gomes, H., and Molholm, S. (2011). The development of audiovisual multisensory integration across childhood and early adolescence: a high-density electrical mapping study. Cereb. Cortex *21*, 1042–1055.

Caruana, F., Jezzini, A., Sbriscia-Fioretti, B., Rizzolatti, G., and Gallese, V. (2011). Emotional and social behaviors elicited by electrical stimulation of the insula in the macaque monkey. Curr. Biol. *21*, 195–199.

Cascio, C.J., Foss-Feig, J.H., Burnette, C.P., Heacock, J.L., and Cosby, A.A. (2012). The rubber hand illusion in children with autism spectrum disorders: delayed influence of combined tactile and visual input on proprioception. Autism *16*, 406–419.

Chaidez, V., Hansen, R.L., and Hertz-Picciotto, I. (2014). Gastrointestinal problems in children with autism, developmental delays or typical development. J. Autism Dev. Disord. *44*, 1117–1127.

Chattopadhyaya, B., Di Cristo, G., Wu, C.Z., Knott, G., Kuhlman, S., Fu, Y., Palmiter, R.D., and Huang, Z.J. (2007). GAD67-mediated GABA synthesis and signaling regulate inhibitory synaptic innervation in the visual cortex. Neuron *54*, 889–903.

Christianson, J.P., Benison, A.M., Jennings, J., Sandsmark, E.K., Amat, J., Kaufman, R.D., Baratta, M.V., Paul, E.D., Campeau, S., Watkins, L.R., et al. (2008). The sensory insular cortex mediates the stress-buffering effects of safety signals but not behavioral control. J. Neurosci. *28*, 13703–13711.

Collignon, O., Charbonneau, G., Peters, F., Nassim, M., Lassonde, M., Lepore, F., Mottron, L., and Bertone, A. (2013). Reduced multisensory facilitation in persons with autism. Cortex *49*, 1704–1710.

Courchesne, E., and Pierce, K. (2005). Why the frontal cortex in autism might be talking only to itself: local over-connectivity but long-distance disconnection. Curr. Opin. Neurobiol. *15*, 225–230.

Craig, A.D. (2009). How do you feel—now? The anterior insula and human awareness. Nat. Rev. Neurosci. *10*, 59–70.

Critchley, H.D., Wiens, S., Rotshtein, P., Ohman, A., and Dolan, R.J. (2004). Neural systems supporting interoceptive awareness. Nat. Neurosci. *7*, 189–195.

Defensor, E.B., Pearson, B.L., Pobbe, R.L., Bolivar, V.J., Blanchard, D.C., and Blanchard, R.J. (2011). A novel social proximity test suggests patterns of social avoidance and gaze aversion-like behavior in BTBR T+ tf/J mice. Behav. Brain Res. *217*, 302–308.

Di Martino, A., Shehzad, Z., Kelly, C., Roy, A.K., Gee, D.G., Uddin, L.Q., Gotimer, K., Klein, D.F., Castellanos, F.X., and Milham, M.P. (2009a). Relationship between cingulo-insular functional connectivity and autistic traits in neurotypical adults. Am. J. Psychiatry *166*, 891–899.

Di Martino, A., Ross, K., Uddin, L.Q., Sklar, A.B., Castellanos, F.X., and Milham, M.P. (2009b). Functional brain correlates of social and nonsocial processes in autism spectrum disorders: an activation likelihood estimation meta-analysis. Biol. Psychiatry *65*, 63–74.

Doyle-Thomas, K.A., Kushki, A., Duerden, E.G., Taylor, M.J., Lerch, J.P., Soorya, L.V., Wang, A.T., Fan, J., and Anagnostou, E. (2013). The effect of diagnosis, age, and symptom severity on cortical surface area in the cingulate cortex and insula in autism spectrum disorders. J. Child Neurol. *28*, 732–739.

Durand, C.M., Betancur, C., Boeckers, T.M., Bockmann, J., Chaste, P., Fauchereau, F., Nygren, G., Rastam, M., Gillberg, I.C., Anckarsäter, H., et al. (2007). Mutations in the gene encoding the synaptic scaffolding protein SHANK3 are associated with autism spectrum disorders. Nat. Genet. *39*, 25–27.

Durand, S., Patrizi, A., Quast, K.B., Hachigian, L., Pavlyuk, R., Saxena, A., Carninci, P., Hensch, T.K., and Fagiolini, M. (2012). NMDA receptor regulation prevents regression of visual cortical function in the absence of Mecp2. Neuron *76*, 1078–1090.

Ebisch, S.J., Gallese, V., Willems, R.M., Mantini, D., Groen, W.B., Romani, G.L., Buitelaar, J.K., and Bekkering, H. (2011). Altered intrinsic functional connectivity of anterior and posterior insula regions in high-functioning participants with autism spectrum disorder. Hum. Brain Mapp. *32*, 1013–1028.

Ellegood, J., Henkelman, R., and Lerch, J.P. (2013). Clustering autism—using neuroanatomical differences in 30 mouse models related to autism to gain insight into the heterogeneity of the disorder. U.S. Soc. Neurosci. Abstr, 692.10.

Engen, H.G., and Singer, T. (2013). Empathy circuits. Curr. Opin. Neurobiol. *23*, 275–282.

Fagiolini, M., and Hensch, T.K. (2000). Inhibitory threshold for critical-period activation in primary visual cortex. Nature *404*, 183–186.

Gick, B., and Derrick, D. (2009). Aero-tactile integration in speech perception. Nature *462*, 502–504.

Gogolla, N., Leblanc, J.J., Quast, K.B., Südhof, T.C., Fagiolini, M., and Hensch, T.K. (2009). Common circuit defect of excitatory-inhibitory balance in mouse models of autism. J. Neurodev. Disord. *1*, 172–181.

Habib, M., Daquin, G., Milandre, L., Royere, M.L., Rey, M., Lanteri, A., Salamon, G., and Khalil, R. (1995). Mutism and auditory agnosia due to bilateral insular damage—role of the insula in human communication. Neuropsychologia *33*, 327–339.

Han, S., Tai, C., Westenbroek, R.E., Yu, F.H., Cheah, C.S., Potter, G.B., Rubenstein, J.L., Scheuer, T., de la Iglesia, H.O., and Catterall, W.A. (2012). Autistic-like behaviour in Scn1a+/- mice and rescue by enhanced GABA-mediated neurotransmission. Nature *489*, 385–390.

Han, K., Holder, J.L., Jr., Schaaf, C.P., Lu, H., Chen, H., Kang, H., Tang, J., Wu, Z., Hao, S., Cheung, S.W., et al. (2013). SHANK3 overexpression causes manic-like behaviour with unique pharmacogenetic properties. Nature *503*, 72–77.

Han, S., Tai, C., Jones, C.J., Scheuer, T., and Catterall, W.A. (2014). Enhancement of inhibitory neurotransmission by GABAA receptors having α2,3-subunits ameliorates behavioral deficits in a mouse model of autism. Neuron *81*, 1282–1289.

Hensch, T.K. (2005). Critical period plasticity in local cortical circuits. Nat. Rev. Neurosci. *6*, 877–888.

Hensch, T.K., and Stryker, M.P. (2004). Columnar architecture sculpted by GABA circuits in developing cat visual cortex. Science *303*, 1678–1681.

Hermans, E.J., van Marle, H.J., Ossewaarde, L., Henckens, M.J., Qin, S., van Kesteren, M.T., Schoots, V.C., Cousijn, H., Rijpkema, M., Oostenveld, R., and Fernández, G. (2011). Stress-related noradrenergic activity prompts large-scale neural network reconfiguration. Science *334*, 1151–1153.

Hsiao, E.Y., McBride, S.W., Hsien, S., Sharon, G., Hyde, E.R., McCue, T., Codelli, J.A., Chow, J., Reisman, S.E., Petrosino, J.F., et al. (2013). Microbiota modulate behavioral and physiological abnormalities associated with neurodevelopmental disorders. Cell *155*, 1451–1463.

Iwai, Y., Fagiolini, M., Obata, K., and Hensch, T.K. (2003). Rapid critical period induction by tonic inhibition in visual cortex. J. Neurosci. *23*, 6695–6702.

Jackson, S.R., Parkinson, A., Kim, S.Y., Schüermann, M., and Eickhoff, S.B. (2011). On the functional anatomy of the urge-for-action. Cogn. Neurosci. *2*, 227–243.

Kouser, M., Speed, H.E., Dewey, C.M., Reimers, J.M., Widman, A.J., Gupta, N., Liu, S., Jaramillo, T.C., Bangash, M., Xiao, B., et al. (2013). Loss of predominant Shank3 isoforms results in hippocampus-dependent impairments in behavior and synaptic transmission. J. Neurosci. *33*, 18448–18468.

Kurth, F., Zilles, K., Fox, P.T., Laird, A.R., and Eickhoff, S.B. (2010). A link between the systems: functional differentiation and integration within the human insula revealed by meta-analysis. Brain Struct. Funct. *214*, 519–534.

Lamm, C., and Singer, T. (2010). The role of anterior insular cortex in social emotions. Brain Struct. Funct. *214*, 579–591.

Lerner, A., Bagic, A., Hanakawa, T., Boudreau, E.A., Pagan, F., Mari, Z., Bara-Jimenez, W., Aksu, M., Sato, S., Murphy, D.L., and Hallett, M. (2009). Involvement of insula and cingulate cortices in control and suppression of natural urges. Cereb. Cortex *19*, 218–223.

Mazurek, M.O., Vasa, R.A., Kalb, L.G., Kanne, S.M., Rosenberg, D., Keefer, A., Murray, D.S., Freedman, B., and Lowery, L.A. (2013). Anxiety, sensory over-responsivity, and gastrointestinal problems in children with autism spectrum disorders. J. Abnorm. Child Psychol. *41*, 165–176.

McElhanon, B.O., McCracken, C., Karpen, S., and Sharp, W.G. (2014). Gastrointestinal Symptoms in Autism Spectrum Disorder: A Meta-analysis. Pediatrics in press.

McFarlane, H.G., Kusek, G.K., Yang, M., Phoenix, J.L., Bolivar, V.J., and Crawley, J.N. (2008). Autism-like behavioral phenotypes in BTBR T+tf/J mice. Genes Brain Behav. *7*, 152–163.

Megnin, O., Flitton, A., Jones, C.R., de Haan, M., Baldeweg, T., and Charman, T. (2012). Audiovisual speech integration in autism spectrum disorders: ERP evidence for atypicalities in lexical-semantic processing. Autism Res. *5*, 39–48.

Menon, V., and Uddin, L.Q. (2010). Saliency, switching, attention and control: a network model of insula function. Brain Struct. Funct. *214*, 655–667.

Moretti, P., and Zoghbi, H.Y. (2006). MeCP2 dysfunction in Rett syndrome and related disorders. Curr. Opin. Genet. Dev. *16*, 276–281.

Nieuwenhuys, R. (2012). The insular cortex: a review. Prog. Brain Res. *195*, 123–163.

O'Neill, M., and Jones, R.S. (1997). Sensory-perceptual abnormalities in autism: a case for more research? J. Autism Dev. Disord. *27*, 283–293.

Olcese, U., Iurilli, G., and Medini, P. (2013). Cellular and synaptic architecture of multisensory integration in the mouse neocortex. Neuron *79*, 579–593.

Onore, C.E., Careaga, M., Babineau, B.A., Schwartzer, J.J., Berman, R.F., and Ashwood, P. (2013). Inflammatory macrophage phenotype in BTBR T+tf/J mice. Front. Neurosci. *7*, 158.

Panksepp, J. (1981). The ontogeny of play in rats. Dev. Psychobiol. *14*, 327–332.

Pearson, B.L., Pobbe, R.L., Defensor, E.B., Oasay, L., Bolivar, V.J., Blanchard, D.C., and Blanchard, R.J. (2011). Motor and cognitive stereotypies in the BTBR T+tf/J mouse model of autism. Genes Brain Behav. *10*, 228–235.

Peça, J., Feliciano, C., Ting, J.T., Wang, W., Wells, M.F., Venkatraman, T.N., Lascola, C.D., Fu, Z., and Feng, G. (2011). Shank3 mutant mice display autistic-like behaviours and striatal dysfunction. Nature *472*, 437–442.

Remedios, R., Logothetis, N.K., and Kayser, C. (2009). An auditory region in the primate insular cortex responding preferentially to vocal communication sounds. J. Neurosci. *29*, 1034–1045.

Rodgers, K.M., Benison, A.M., Klein, A., and Barth, D.S. (2008). Auditory, somatosensory, and multisensory insular cortex in the rat. Cereb. Cortex *18*, 2941–2951.

Rubenstein, J.L., and Merzenich, M.M. (2003). Model of autism: increased ratio of excitation/inhibition in key neural systems. Genes Brain Behav. *2*, 255–267.

Russo, N., Foxe, J.J., Brandwein, A.B., Altschuler, T., Gomes, H., and Molholm, S. (2010). Multisensory processing in children with autism: high-density electrical mapping of auditory-somatosensory integration. Autism Res. *3*, 253–267.

Sawatari, H., Tanaka, Y., Takemoto, M., Nishimura, M., Hasegawa, K., Saitoh, K., and Song, W.J. (2011). Identification and characterization of an insular auditory field in mice. Eur. J. Neurosci. *34*, 1944–1952.

Scattoni, M.L., Ricceri, L., and Crawley, J.N. (2011). Unusual repertoire of vocalizations in adult BTBR T+tf/J mice during three types of social encounters. Genes Brain Behav. *10*, 44–56.

Shibuki, K., Hishida, R., Murakami, H., Kudoh, M., Kawaguchi, T., Watanabe, M., Watanabe, S., Kouuchi, T., and Tanaka, R. (2003). Dynamic imaging of somatosensory cortical activity in the rat visualized by flavoprotein autofluorescence. J. Physiol. *549*, 919–927.

Silani, G., Bird, G., Brindley, R., Singer, T., Frith, C., and Frith, U. (2008). Levels of emotional awareness and autism: an fMRI study. Soc. Neurosci. *3*, 97–112.

Stein, B.E., and Stanford, T.R. (2008). Multisensory integration: current issues from the perspective of the single neuron. Nat. Rev. Neurosci. *9*, 255–266.

Takemoto, M., Hasegawa, K., Nishimura, M., and Song, W.J. (2014). The insular auditory field receives input from the lemniscal subdivision of the auditory thalamus in mice. J. Comp. Neurol. *522*, 1373–1389.

Uddin, L.Q., and Menon, V. (2009). The anterior insula in autism: under-connected and under-examined. Neurosci. Biobehav. Rev. *33*, 1198–1203.

von dem Hagen, E.A., Stoyanova, R.S., Baron-Cohen, S., and Calder, A.J. (2013). Reduced functional connectivity within and between 'social' resting state networks in autism spectrum conditions. Soc. Cogn. Affect. Neurosci. *8*, 694–701.

Wallace, M.T., Carriere, B.N., Perrault, T.J., Jr., Vaughan, J.W., and Stein, B.E. (2006). The development of cortical multisensory integration. J. Neurosci. *26*, 11844–11849.

Wang, X., McCoy, P.A., Rodriguiz, R.M., Pan, Y., Je, H.S., Roberts, A.C., Kim, C.J., Berrios, J., Colvin, J.S., Bousquet-Moore, D., et al. (2011). Synaptic dysfunction and abnormal behaviors in mice lacking major isoforms of Shank3. Hum. Mol. Genet. *20*, 3093–3108.

Wylie, K.P., and Tregellas, J.R. (2010). The role of the insula in schizophrenia. Schizophr. Res. *123*, 93–104.

Yang, M., Bozdagi, O., Scattoni, M.L., Wöhr, M., Roullet, F.I., Katz, A.M., Abrams, D.N., Kalikhman, D., Simon, H., Woldeyohannes, L., et al. (2012). Reduced excitatory neurotransmission and mild autism-relevant phenotypes in adolescent Shank3 null mutant mice. J. Neurosci. *32*, 6525–6541.